Inverse Problems 5 (1989) 441–461. Printed in Great Britain

Super-resolution in confocal scanning microscopy: II. The incoherent case

M Bertero†, P Boccacci†, M Defrise‡§, C De Mol‖§ and E R Pike¶

† Dipartimento di Fisica dell'Università di Genova and Istituto Nazionale di Fisica Nucleare, Via Dodecaneso 33, I-16146 Genova, Italy

‡ Radioisotopen, Akademisch Ziekenhuis, Vrije Universiteit Brussel, B-1090 Brussel, Belgium

‖ Département de Mathématique, Université Libre de Bruxelles, B-1050 Bruxelles, Belgium

¶ Department of Physics, King's College, London WC2R 2LS, UK and RSRE, Great Malvern, WR14 3PS, UK

Received 24 January 1989

Abstract. In several previous papers we have shown that the resolution of a confocal scanning microscope can be improved by recording the full image at each scanning point and then inverting the data. These analyses were restricted to the case of coherent illumination. In this paper we investigate, along similar lines, the incoherent case, which applies to fluorescence microscopy. We investigate the one-dimensional and two-dimensional square-pupil problems and we prove, by means of numerical computations of the singular value spectrum and of the impulse response function, that for a signal-to-noise ratio of, say, 10%, it is possible to obtain an improvement of approximately 60% in resolution with respect to the conventional incoherent light confocal microscope. This represents a working bandwidth of 3.5 times the Rayleigh limit.

1. Introduction

In a previous paper ([1], hereafter referred to as I) we have investigated the improvement in resolution (super-resolution) which can be obtained in confocal scanning light microscopy (CSLM) when the full image is detected at each step of the scanning procedure. We recall that in the usual CSLM the image is detected only on the optical axis and that the two-dimensional image is the result of the two-dimensional scanning. In I the analysis was restricted to the coherent case. In this paper we investigate, along parallel lines, the case of incoherent imaging.

Incoherent CSLM applies to the imaging of fluorescent objects. In such a case the intensity of the fluorescent light is proportional to the intensity of the incident radiation. Then it is easy to show that, when the primary and the fluorescent wavelengths essentially coincide, the bandwidth of the usual instrument is four times the bandwidth of the conventional coherent microscope. The improvement in resolution, however, is only a factor of 1.8 times the classical Rayleigh resolution distance [2].

§ M Defrise and C De Mol are respectively 'Bevoegdverklaard Navorser' and 'Chercheur qualifié' of the Belgian National Fund for Scientific Research.

0266-5611/89/040441+21

This is a consequence of the behaviour of the transfer function of the instrument, which tends to zero very rapidly at the edges of the band. In other words, the highest Fourier components of the object in this band are not transmitted in practice by the instrument. In order to increase the information about these components, one can consider a modification of the microscope such as that considered in I. This consists of detecting the full image at any scanning position and in using data inversion methods for recovering the transmitted components of the object. In the following we will call *conventional* CSLM the well established technique where the image is detected only on the optical axis and *super-resolving* CSLM the new technique where the full image is determined by means of a suitable array of detectors. We point out that this new technique does not modify the transmitted band but introduces a considerable improvement of the transfer function [3].

If $f(\boldsymbol{x})$ is the distribution of the fluorescent centres in the focal plane and if $S_1(\boldsymbol{x})$, $S_2(\boldsymbol{x})$ are the point-spread functions of the illuminating and of the imaging lenses, respectively, then, assuming complete incoherence of the fluorescent radiation, the basic relationship between the object $f(\boldsymbol{x})$ and the intensity distribution $g(\boldsymbol{x})$ in the image plane is

$$g(\boldsymbol{x}) = \int |S_2(\boldsymbol{x}-\boldsymbol{y})|^2 |S_1(\boldsymbol{y})|^2 f(\boldsymbol{y})\, d\boldsymbol{y}. \tag{1.1}$$

Notice that, even in the reflection mode of operation [4], the two point-spread functions do not coincide because the primary and the fluorescent wavelengths are different. This effect, however, is not large—of the order of 10%—and it can be neglected in the first approximation.

In this paper the basic relationship will be (1.1). This means that we do not consider here one of the most interesting properties of fluorescence CSLM, i.e. the possibility of obtaining a three-dimensional image of the sample by means of three-dimensional scanning [4, 5]. Also in this case one can investigate the improvement in resolution provided by super-resolving CSLM. This will be the subject of future studies. Here, as in I, we restrict the analysis to two-dimensional objects or, more precisely, to objects whose size along the optical axis is of the order of the axial resolution (approximately $1\,\mu$m). As a consequence we only investigate the improvement in lateral resolution.

We briefly discuss now the relationship between the basic equation of conventional CSLM and that of super-resolving CSLM. The scanning of the sample consists of considering all the possible translations of the sample itself. Now, to a translation $-\boldsymbol{\xi}$ there corresponds a new object $f(\boldsymbol{x}+\boldsymbol{\xi})$ and a new image $g(\boldsymbol{\xi}, \boldsymbol{x})$ which, as follows from (1.1), is given by

$$g(\boldsymbol{\xi}, \boldsymbol{x}) = \int |S_1(\boldsymbol{x}-\boldsymbol{y})|^2 |S_2(\boldsymbol{y})|^2 f(\boldsymbol{y}+\boldsymbol{\xi})\, d\boldsymbol{y}. \tag{1.2}$$

In conventional CSLM the image is recorded only on the optical axis, i.e. $\boldsymbol{x}=0$. Then, if we neglect the finite size of the pinhole, if we ignore the difference between the two point-spread functions, i.e. $S_1(\boldsymbol{x}) = S_2(\boldsymbol{x}) = S(\boldsymbol{x})$, and if we assume that $S(\boldsymbol{x})$ is an even function, then (1.2) implies that the image provided by conventional CSLM is

$$G(\boldsymbol{\xi}) = \int |S(\boldsymbol{\xi}-\boldsymbol{y})|^4 f(\boldsymbol{y})\, d\boldsymbol{y}. \tag{1.3}$$

where $G(\boldsymbol{\xi}) = g(\boldsymbol{\xi}, 0)$.

On the other hand, in super-resolving CSLM the full image $g(\xi, x)$ is detected for any given ξ (of course, in practice, only a finite set of values of $g(\xi, x)$ is measured). Then (1.2) is an integral equation which must be solved to determine $f(y+\xi)$. As is obvious, it is sufficient to recover the object at $y=0$ since this value is just $f(\xi)$. More precisely, we do not obtain the exact value of $f(\xi)$ but an approximation to it, which will be denoted by $\tilde{f}(\xi)$. This approximation is the image provided by super-resolving CSLM and this must be compared with the image $G(\xi)$ provided by conventional CSLM.

The solution of (1.2) implies the inversion of an integral operator and an important fact is that this operator is the same for any scanning position. As a consequence, the inversion algorithm is also independent of the scanning position.

As in I we first consider in detail the one-dimensional problem. In such a case, if we take the Rayleigh distance associated with the two identical lenses as length unit and if we assume that the lenses are ideal low-pass filters, then the appropriate integral equation can be written in the form

$$g = Af \tag{1.4}$$

where

$$(Af)(x) = \int_{-\infty}^{+\infty} \operatorname{sinc}^2(x-y) \operatorname{sinc}^2(y) f(y)\, dy \tag{1.5}$$

and

$$\operatorname{sinc}(x) = \frac{\sin(\pi x)}{\pi x}. \tag{1.6}$$

In §§2 and 3 we investigate several mathematical properties of the integral operator (1.5) which are relevant to the solution of (1.4). Since the basic tool is the singular system of the operator (1.5), in §4 we describe a numerical method for the determination of such a system. This method consists of discretising the integral equation using the well known sampling expansion of band-limited functions. The numerical results obtained by means of this method are discussed in §5. In §6 we determine the impulse response function and the transfer function of the super-resolving CSLM and in this way we determine the improvement in resolution with respect to the conventional CSLM. Finally in §7 we extend the results to the two-dimensional problem in the case of square pupils.

2. The one-dimensional integral operator

As we discussed in §1, we must investigate the following problem. Given the image $g(x)$, find the value at $y=0$ of the solution $f(y)$ of (1.4) and (1.5).

The existence and uniqueness of the solution of this problem are related respectively to the structure of the range and of the null space of the integral operator (1.5). In fact, a solution of (1.4) exists if and only if g belongs to the range of A, denoted by $R(A)$. This set will be called the set of the *noise-free images*. Moreover the solution of (1.4) is unique if and only if the null space of A, denoted by $N(A)$, is trivial, i.e. if it coincides with the null element of the space. If $N(A)$ is not trivial, then it is called the

subspace of *invisible objects*, since the elements of $N(A)$ produce an image which is zero everywhere.

We assume that both objects and images are elements of $L^2(-\infty, +\infty)$. Then our first result is the following: the range of A is dense in the subspace of the band-limited functions with bandwidth 2π. The proof is as follows. From (1.4) and (1.5) it is obvious that a function $g \in R(A)$ must be band limited with bandwidth 2π. Therefore, in order to prove the result it is sufficient to prove that if a band-limited function $\psi(x)$ with bandwidth 2π is orthogonal to $R(A)$, then $\psi = 0$. Now, if $\psi(x)$ is such that $(\psi, Af) = 0$ for any $f \in L^2(-\infty, +\infty)$, this implies that $A^*\psi = 0$, where A^* is the adjoint operator given by

$$(A^*g)(y) = \operatorname{sinc}^2(y) \int_{-\infty}^{+\infty} \operatorname{sinc}^2(x-y) g(x)\, dx. \tag{2.1}$$

Since the function $\operatorname{sinc}^2(y)$ is different from zero almost everywhere, the equation $A^*\psi = 0$ is equivalent to

$$\int_{-\infty}^{+\infty} \operatorname{sinc}^2(y-x)\psi(x)\, dx = 0. \tag{2.2}$$

Now, the Fourier transform of the function $s(x) = \operatorname{sinc}^2(x)$ is

$$\hat{s}(\omega) = \begin{cases} 1 - (1/2\pi)|\omega| & |\omega| < 2\pi \\ 0 & |\omega| > 2\pi \end{cases} \tag{2.3}$$

and therefore from (2.2) we derive $\hat{s}(\omega)\hat{\psi}(\omega) = 0$ everywhere. It follows that $\hat{\psi}(\omega) = 0$ when $|\omega| < 2\pi$ and, since $\psi(x)$ is band limited with bandwidth 2π, it also follows that $\psi(x) = 0$ everywhere. This completes the proof of the result.

The previous result implies that a noisy image, in general, does not belong to $R(A)$ (the noise may not be band limited) and in such a case the solution of (1.4) does not exist. In other words, the problem is ill posed and one must use well established techniques, such as regularisation methods, truncated singular function expansions etc [6] in order to find stable approximate solutions.

As concerns the null space $N(A)$, a complete characterisation will be given in § 3. Here we just point out that $N(A)$ is not trivial and therefore the solution of (1.4) is not unique. Now, an arbitrary object $f(y)$ can be uniquely decomposed into a component on $N(A)$, its invisible component, and a component orthogonal to $N(A)$, its transmitted component.

It is obvious that, given the image g, we can at most recover the transmitted component of the object. The latter is a band-limited function with bandwidth 4π, as follows from (2.1) if we recall that the orthogonal complement of $N(A)$ coincides with the closure of the range of A^*. This result justifies the statement contained in § 1, namely that the bandwidths of super-resolving CSLM and conventional CSLM coincide.

Another basic property of the operator (1.5) is compactness. More precisely, the operator A is of the Hilbert–Schmidt class [7] since its kernel is a square-integrable function. Then we can introduce the singular system of A, i.e. the set of the triples $\{\alpha_k; u_k, v_k\}_{k=0}^{\infty}$ which solve the coupled homogeneous equations

$$Au_k = \alpha_k v_k \qquad A^*v_k = \alpha_k u_k. \tag{2.4}$$

As usual, the singular values α_k are ordered in such a way that they form a decreasing sequence.

From general properties of the singular functions u_k, v_k and from the results derived above we can make the following deductions.

(i) The singular functions u_k form an orthonormal basis in the orthogonal complement of $N(A)$; they are band-limited function with bandwidth 4π and they have double zeros at the integer sampling points.

(ii) The singular functions v_k are band-limited functions with bandwidth 2π and they form an orthonormal basis in the closure of $R(A)$.

The singular system of the operator A provides a representation of the *generalised solution* of (1.4). As is well known, this is a least-squares solution of minimal norm [8]. It is always unique and it exists when g is a noise-free image. Another basic property of the generalised solution, denoted by $f^{\dagger}(y)$, is that it is orthogonal to $N(A)$. Therefore the generalised solution coincides with the transmitted component of the object. Its expansion in terms of singular functions is [9]

$$f^{\dagger}(y) = \sum_{k=0}^{+\infty} \frac{1}{\alpha_k}(g, v_k)u_k(y) \tag{2.5}$$

where (g, v_k) denotes the usual scalar product of $L^2(-\infty, +\infty)$.

Since we are only interested in the value of $f^{\dagger}(y)$ at $y=0$, in the case of noise-free data $g=Af$, from the relation

$$(g, v_k) = (Af, v_k) = (f, A^* v_k) = \alpha_k(f, u_k) \tag{2.6}$$

we obtain

$$f^{\dagger}(0) = \int_{-\infty}^{+\infty} T(y)f(y)\,dy \tag{2.7}$$

where

$$T(y) = \sum_{k=0}^{+\infty} u_k(0)u_k(y). \tag{2.8}$$

If we take into account now the effect of the scanning, i.e. if we replace $f(y)$ by $f(y+\xi)$, if we denote by $f^{\dagger}(\xi, y)$ the corresponding generalised solution and if we put $\tilde{f}(\xi) = f^{\dagger}(\xi, 0)$, then we get

$$\tilde{f}(\xi) = \int_{-\infty}^{+\infty} T(\xi - y)f(y)\,dy. \tag{2.9}$$

This is the image provided by super-resolving CSLM, in the case of noise-free data, and it must be compared with the image (1.3) of conventional CSLM, which in the present case becomes

$$G(\xi) = \int_{-\infty}^{+\infty} \mathrm{sinc}^4(\xi - y)f(y)\,dy. \tag{2.10}$$

This point will be discussed in §6.

3. The null space of the one-dimensional operator

In this section we derive a characterisation of the null space of the integral operator (1.5), which will be used for the solution of the following problem: given an arbitrary object $f(y)$, determine its invisible component, i.e. its projection onto $N(A)$.

We first notice that $N(A)$ contains all the functions whose Fourier transform is zero over the band $[-4\pi, 4\pi]$. This subset will be denoted by $N_0(A)$. Therefore the interesting part of $N(A)$ is the subspace of the functions with bandwidth 4π. More precisely, we must investigate the solutions of the equation $A\phi = 0$ assuming that ϕ is band limited with bandwidth 4π. This subset will be denoted by $N_1(A)$ so that we have $N(A) = N_0(A) \oplus N_1(A)$.

If $\hat{s}(\omega)$ is the function defined in (2.3) then, by taking the Fourier transform of both sides of the equation $A\phi = 0$, we get

$$\hat{s}(\omega) \int_{-\infty}^{+\infty} \hat{s}(\omega - \omega')\hat{\phi}(\omega')\, d\omega' = 0. \tag{3.1}$$

This equation is non-trivial only on the interval $|\omega| < 2\pi$. Since on such an interval $\hat{s}(\omega) \neq 0$ and since $\hat{\phi}(\omega') \neq 0$ only when $|\omega'| < 4\pi$, it follows that

$$\int_{-4\pi}^{4\pi} \hat{s}(\omega - \omega')\hat{\phi}(\omega')\, d\omega' = 0 \qquad |\omega| < 2\pi. \tag{3.2}$$

This equation can be written in a more explicit form using (2.3). We obtain

$$\int_{\omega-2\pi}^{\omega} \left(1 - \frac{\omega - \omega'}{2\pi}\right) \hat{\phi}(\omega')\, d\omega' + \int_{\omega}^{\omega+2\pi} \left(1 + \frac{\omega - \omega'}{2\pi}\right) \hat{\phi}(\omega')\, d\omega' = 0 \qquad |\omega| < 2\pi \tag{3.3}$$

and, by a change of variable in the second integral, we find

$$\int_{\omega-2\pi}^{\omega} \hat{\phi}(\omega')\, d\omega' + \int_{\omega-2\pi}^{\omega} \frac{\omega - \omega'}{2\pi} (\hat{\phi}(\omega' + 2\pi) - \hat{\phi}(\omega'))\, d\omega' = 0 \qquad |\omega| < 2\pi. \tag{3.4}$$

Now, let us denote by $\psi(\omega)$ the left-hand side of (3.4). Then one easily obtains that

$$\psi'(\omega) = \frac{1}{2\pi} \int_{\omega-2\pi}^{\omega} (\hat{\phi}(\omega' + 2\pi) - \hat{\phi}(\omega'))\, d\omega' \qquad |\omega| < 2\pi. \tag{3.5}$$

Since $\psi'(\omega)$ is absolutely continuous, the second derivative $\psi''(\omega)$ exists almost everywhere and is given by

$$\psi''(\omega) = \hat{\phi}(\omega + 2\pi) - 2\hat{\phi}(\omega) + \hat{\phi}(\omega - 2\pi) \qquad |\omega| < 2\pi. \tag{3.6}$$

Finally, if we observe that the original condition $\psi(\omega) = 0$, $|\omega| < 2\pi$, is equivalent to the following set of conditions:

$$\psi''(\omega) = 0, |\omega| < 2\pi \qquad \psi'(0) = 0 \qquad \psi(0) = 0 \tag{3.7}$$

then we conclude that $N_1(A)$ is the set of all the functions ϕ satisfying the conditions

$$2\hat{\phi}(\omega) - \hat{\phi}(\omega + 2\pi) - \hat{\phi}(\omega - 2\pi) = 0 \qquad |\omega| < 2\pi \tag{3.8}$$

$$\int_{0}^{2\pi} \hat{\phi}(\omega')\, d\omega' = \int_{-2\pi}^{0} \hat{\phi}(\omega')\, d\omega' \tag{3.9}$$

$$\int_{-2\pi}^{2\pi} \hat{\phi}(\omega')\,\mathrm{d}\omega' = \frac{1}{2\pi}\int_{0}^{2\pi} \omega'\hat{\phi}(\omega')\,\mathrm{d}\omega' - \frac{1}{2\pi}\int_{-2\pi}^{0} \omega'\hat{\phi}(\omega')\,\mathrm{d}\omega'. \tag{3.10}$$

Condition (3.9) is just $\psi'(0)=0$, while condition (3.10) is $\psi(0)=0$.

We notice that the conditions (3.9) and (3.10) involve only the value of $\hat{\phi}(\omega)$ on the interval $[-2\pi, 2\pi]$ while condition (3.8) gives essentially the continuation of $\hat{\phi}(\omega)$ from the interval $[-2\pi, 2\pi]$ into the intervals $[-4\pi, -2\pi]$ and $[2\pi, 4\pi]$. Therefore, let us denote by $\hat{\alpha}(\omega)$ the values of $\hat{\phi}(\omega)$ on the interval $[-2\pi, 2\pi]$. This is a square-integrable function which is arbitrary except for being subjected to conditions (3.9) and (3.10). The latter can now be written in the following form:

$$\int_{-2\pi}^{2\pi} \varepsilon(\omega')\hat{\alpha}(\omega')\,\mathrm{d}\omega' = 0 \tag{3.11}$$

$$\int_{-2\pi}^{2\pi} \left(1 - \frac{1}{2\pi}\varepsilon(\omega')\omega'\right)\hat{\alpha}(\omega')\,\mathrm{d}\omega' = 0 \tag{3.12}$$

where $\varepsilon(\omega')$ denotes the sign of ω'. Then (3.8) with $\omega \in (-2\pi, 0)$ gives the values of $\hat{\phi}(\omega)$ in the interval $(-4\pi, -2\pi)$ while the same equation with $\omega \in (0, 2\pi)$ gives the values of $\hat{\phi}(\omega)$ in the interval $(2\pi, 4\pi)$.

The final result can be formulated as follows: the null space $N(A)$ is given by the direct sum $N(A) = N_0(A) \oplus N_1(A)$ where $N_0(A)$ is the set of all the functions ϕ whose Fourier transform is zero over the interval $[-4\pi, 4\pi]$ while $N_1(A)$ is the set of all the band-limited functions ϕ, with bandwidth 4π, whose Fourier transform is given by

$$\hat{\phi}(\omega) = \begin{cases} 2\hat{\alpha}(\omega + 2\pi) - \hat{\alpha}(\omega + 4\pi) & -4\pi < \omega < -2\pi \\ \hat{\alpha}(\omega) & -2\pi < \omega < 2\pi \\ 2\hat{\alpha}(\omega - 2\pi) - \hat{\alpha}(\omega - 4\pi) & 2\pi < \omega < 4\pi \end{cases} \tag{3.13}$$

where $\hat{\alpha}(\omega)$ is an arbitrary function of $L^2(-2\pi, 2\pi)$ satisfying conditions (3.11) and (3.12).

We notice that, as one can easily check, (3.4) is satisfied by all the functions $\hat{\phi}_n(\omega) = \exp(in\omega)$, $|\omega| < 4\pi$, with $n \neq 0$. From the sampling theorem it follows that $N_1(A)$ contains all the band-limited functions with bandwidth 4π whose sampling values are different from zero only at the sampling points $x_n = n$, with $n = \pm 1, \pm 2, \ldots$. The subspace of these functions, however, does not coincide with $N_1(A)$ but is a proper subset of $N_1(A)$.

We can now solve the problem stated at the beginning of the section. In fact, let $f(y)$ be an arbitrary object and let $\hat{f}(\omega)$ be its Fourier transform. If we denote by $\hat{f}_0(\omega)$ the function which coincides with $\hat{f}(\omega)$ for $|\omega| > 4\pi$ and which is zero for $|\omega| < 4\pi$, then $f_0 \in N_0(A)$. Therefore, in order to completely determine the invisible component of $f(y)$, we must determine the projection onto $N_1(A)$ of the restriction of $\hat{f}(\omega)$ to the interval $[-4\pi, 4\pi]$. This projection can be determined by looking for a function $\hat{\phi}$ which satisfies conditions (3.13), (3.11), (3.12) and which is a solution of the following variational problem:

$$\int_{-4\pi}^{4\pi} |\hat{f}(\omega) - \hat{\phi}(\omega)|^2\,\mathrm{d}\omega = \text{minimum}. \tag{3.14}$$

This is a constrained minimisation problem for the function $\hat{\alpha}(\omega)$ and it can be solved in a standard way using the method of Lagrange multipliers. Since the

constraints are provided by (3.11) and (3.12), the constrained problem (3.14) can be replaced by the following unconstrained problem:

$$\int_{-4\pi}^{4\pi} |\hat{f}(\omega)-\hat{\phi}(\omega)|^2\,\mathrm{d}\omega + 2\lambda\int_{-2\pi}^{2\pi}\varepsilon(\omega)\hat{a}(\omega)\,\mathrm{d}\omega + 2\mu\int_{-2\pi}^{2\pi}\left(1-\frac{1}{2\pi}\omega\varepsilon(\omega)\right)\hat{a}(\omega)\,\mathrm{d}\omega$$
$$= \text{minimum} \tag{3.15}$$

where $\hat{\phi}(\omega)$ is given in terms of $\hat{a}(\omega)$ according to (3.13). This problem must be solved for any value of the Lagrange multipliers λ and μ and the values of these parameters must be chosen in order to satisfy conditions (3.11) and (3.12).

If one considers separately the variation of $\hat{a}(\omega)$ when $\omega\in(0, 2\pi)$ and the variation of $\hat{a}(\omega)$ when $\omega\in(-2\pi, 0)$, then after some elementary but lengthy computations one finds that the minimum of the functional (3.15) is given by

$$\hat{a}(\omega)=\tfrac{1}{10}\{4\hat{f}(\omega-2\pi)+3\hat{f}(\omega)+2\hat{f}(\omega+2\pi)+\hat{f}(\omega+4\pi)+\lambda-\mu[3+(1/2\pi)\omega]\}$$
$$\omega<0 \tag{3.16}$$

$$\hat{a}(\omega=\tfrac{1}{10}\{4\hat{f}(\omega+2\pi)+3\hat{f}(\omega)+2\hat{f}(\omega-2\pi)+\hat{f}(\omega-4\pi)-\lambda-\mu[3-(1/2\pi)\omega]\}$$
$$\omega>0. \tag{3.17}$$

If we now insert (3.16) and (3.17) into (3.11) and (3.12) we easily recognise that λ is determined by (3.11) while μ is determined by (3.12). The result is

$$\lambda=(1/4\pi)(3I_4+I_3-I_2-3I_1) \tag{3.18}$$

$$\mu=(3/16\pi)(7I_4+3I_3+3I_2+7I_1-3J_4-J_3+J_2+3J_1) \tag{3.19}$$

where

$$I_j=\int_{-4\pi+2\pi(j-1)}^{-4\pi+2\pi j}\hat{f}(\omega)\,\mathrm{d}\omega \qquad j=1,2,3,4 \tag{3.20}$$

$$J_j=\frac{1}{2\pi}\int_{-4\pi+2\pi(j-1)}^{-4\pi+2\pi j}\omega\hat{f}(\omega)\,\mathrm{d}\omega \qquad j=1,2,3,4. \tag{3.21}$$

These formulae solve completely the problem of determining the invisible component of an arbitrary object $f(y)$. In particular they will be used in §6 for determining the impulse response function (2.8).

4. Discretisation of the integral equation

A basic property of the integral operator related to the one-dimensional coherent problem is that its singular values and singular functions have very simple analytic expressions [10]. As a consequence they can be easily computed with any desired degree of accuracy. Moreover, as proved in I using sampling expansions both for the image and for the object, the determination of the generalised inverse of the coherent integral operator is equivalent to the inversion of an infinite-dimensional matrix. This equivalence is used in I for investigating the problem with discrete data and for computing its singular system. In a subsequent paper [11] it was shown that the inverse of the infinite-dimensional matrix also has a very simple analytic expression. As far as we know, similar results do not hold true in the incoherent case and therefore we must

find a numerical approach for the determination of the singular system of the integral operator (1.5).

In this section we describe in detail a method based on sampling expansions, which is an extension of the method introduced in I and which has already been briefly discussed in [12].

If $g(x)$ is an image in the range of the operator (1.5) (noise-free image) then, as proved in §2, $g(x)$ is a band-limited function with bandwidth 2π. As a consequence it can be represented by means of the sampling expansion

$$g(x)=\sum_{n=-\infty}^{+\infty} g(x_n)\,\mathrm{sinc}[2(x-x_n)] \tag{4.1}$$

where

$$x_n=n/2 \qquad n=0,\ \pm1,\ \pm2,\ \ldots \tag{4.2}$$

and the following equality holds true:

$$\int_{-\infty}^{+\infty}|g(x)|^2\,\mathrm{d}x=\frac{1}{2}\sum_{n=-\infty}^{+\infty}|g(x_n)|^2. \tag{4.3}$$

As concerns the generalised solution (1.4), it is an element of $N(A)^{\perp}$, the orthogonal complement of the null space of A, and therefore we can restrict A to $N(A)^{\perp}$. The elements of $N(A)^{\perp}$ are band-limited functions with bandwidth 4π and they have zeros at the integer sampling points, except $y=0$, i.e. $f(m)=0$ if $m=\pm1,\ \pm2,\ldots$. These properties follow from the results of §3. As a consequence $f(y)$ can be represented by means of the sampling expansion

$$f(y)=\sum_{m=-\infty}^{+\infty} f(y_m)\,\mathrm{sinc}[4(y-y_m)] \tag{4.4}$$

where $y_0=0$, $y_{\pm1}=\pm\frac{1}{4}$, $y_{\pm2}=\pm\frac{2}{4}$, $y_{\pm3}=\pm\frac{3}{4}$, $y_{\pm4}=\pm\frac{5}{4}$, etc. In general, for $m\neq0$

$$m=\pm(3k+j) \qquad y_m=\pm(k+j/4) \qquad k=0,1,2,\ldots,j=1,2,3. \tag{4.5}$$

Equality (4.3) is replaced by

$$\int_{-\infty}^{+\infty}|f(y)|^2\,\mathrm{d}y=\frac{1}{4}\sum_{m=-\infty}^{+\infty}|f(y_m)|^2. \tag{4.6}$$

If we now consider (1.4) at the point x_n and if we use the expansion (4.4) for $f(y)$, we find

$$g(x_n)=\sum_{m=-\infty}^{+\infty} C_{nm}f(y_m) \qquad n=0,\ \pm1,\ldots \tag{4.7}$$

where

$$C_{nm}=\int_{-\infty}^{+\infty}\mathrm{sinc}^2(y-x_n)\,\mathrm{sinc}^2(y)\,\mathrm{sinc}[4(y-y_m)]\,\mathrm{d}y. \tag{4.8}$$

If we notice that the functions $k_n(y) = \operatorname{sinc}^2(y - x_n)\operatorname{sinc}^2(y)$ are band limited with bandwidth 4π and if we use the projection properties of the sampling functions $\operatorname{sinc}[4(y - y_m)]$, we get

$$C_{nm} = \tfrac{1}{4}\operatorname{sinc}^2(x_n - y_m)\operatorname{sinc}^2(y_m). \tag{4.9}$$

As follows from (4.2) and (4.5), it is convenient to introduce the coefficients

$$b_n = (1/\sqrt{2})g(x_n) \qquad a_m = \tfrac{1}{2}f(y_m). \tag{4.10}$$

Then the L^2-norms of the functions $g(x)$ and $f(y)$ coincide with the l^2-norms (sum of squares) of the sequences $\{b_n\}_{n=-\infty}^{+\infty}$ and $\{a_m\}_{m=-\infty}^{+\infty}$ respectively.

In terms of the coefficients (4.10) the infinite-dimensional linear system (4.7) takes the form

$$b_n = \sum_{m=-\infty}^{+\infty} A_{nm}a_m \qquad n = 0, \pm 1, \ldots \tag{4.11}$$

where

$$A_{nm} = (1/2^{3/2})\operatorname{sinc}^2(x_n - y_m)\operatorname{sinc}^2(y_m). \tag{4.12}$$

We notice that the inverse of this infinite-dimensional matrix does not exist. In fact this matrix is isomorphic to the restriction of the integral operator (1.5) to the subspace of band-limited functions represented by the expansion (4.4). Since this subspace is broader than $N(A)^{\perp}$, the null space of the restricted integral operator is not trivial.

The infinite-dimensional matrix (4.12) has exactly the same singular values as the integral operator (1.5). Moreover, if α_k is one of the singular values and if $\{u_{k,m}\}_{m=-\infty}^{+\infty}$, $\{v_{k,n}\}_{n=-\infty}^{+\infty}$ are the singular sequences associated with this singular value, the corresponding singular functions of the integral operator (1.5) are obtained by means of (4.1), (4.4) and (4.10):

$$u_k(y) = 2\sum_{m=-\infty}^{+\infty} u_{k,m}\operatorname{sinc}[4(y - y_m)] \tag{4.13}$$

$$v_k(x) = \sqrt{2}\sum_{n=-\infty}^{+\infty} v_{k,n}\operatorname{sinc}[2(x - x_n)]. \tag{4.14}$$

Approximations of the singular values and singular functions can be obtained by considering finite sections of the infinite-dimensional matrix (4.12).

5. Numerical results

The discretisation of the basic integral equation, as described in the previous section, is an extension of the method proposed in I for the coherent problem. In I it is shown that the method can provide excellent approximations of the largest singular values (we recall that the exact values are known from the result of Gori and Guattari [10]), using a rather small number of sampling points for the image and a sufficiently large number of sampling points for the object. This result has important practical implications. Since only the largest singular values are important for practical data

inversion, it means that the problem with continuous data is practically equivalent to a problem with a small number of discrete data. It is interesting to verify whether a similar result holds true also in the incoherent case.

Let us denote by $A_{nm}^{(N,M)}$ the section of the infinite-dimensional matrix (4.12) which is obtained by taking $n=0, \pm 1, \ldots, \pm N$; $m=0, \pm 1, \ldots, \pm M$. We put

$$N_0 = 2N+1 \qquad M_0 = 2M+1. \tag{5.1}$$

We recall that the sampling distance is $\frac{1}{2}$ for the image and $\frac{1}{4}$ for the object (the Rayleigh distance is the unit of length). Therefore, if N is even, N_0 sampling points corresponds to the interval $[-N/2, N/2]$ in the image space. As concerns the sampling of the object, we recall that we have only three sampling points inside any unit interval. Then, if M is a multiple of 3, M_0 sampling points corresponds to the interval $[-M/3, M/3]$ in the object space. In other words, the integral from $-\infty$ to $+\infty$ in (1.5) is approximated by the integral extended to $[-M/3, M/3]$. For example, $M_0=97$ corresponds to $[-16, 16]$.

The matrix $A_{nm}^{(N,M)}$ is a $N_0 \times M_0$ matrix. In general it is not a square matrix since we do not take the same number of sampling points for the image and the object. Its singular values provide approximations of the largest singular values of the infinite matrix (4.12). In fact, in the limit $N \to \infty$, $M \to \infty$, the singular values of $A_{nm}^{(N,M)}$ converge to the singular values of A_{nm}, as follows from standard results of perturbation theory [13]. The matrix $A_{nm}^{(N,M)}$ can be considered, indeed, as a perturbation of A_{nm}, obtained by annihilating the matrix elements of A_{nm} with $|n|>N$ and/or $|m|>M$. Analogously the singular vectors of $A_{nm}^{(N,M)}$ provide approximations of the singular vectors (sequences) of A_{nm}. The corresponding approximations of the singular functions of the integral operator (1.5) are obtained by truncating the expansions (4.13) and (4.14). For example, in the case of the singular functions $u_k(y)$, we have the approximation

$$u_k^{(N,M)}(y) = 2 \sum_{m=-M}^{M} u_{k,m}^{(N,M)} \operatorname{sinc}[4(y-y_m)] \tag{5.2}$$

where $\{u_{k,m}^{(N,M)}\}_{m=-M}^{M}$ is the singular vector of the matrix $A_{nm}^{(N,M)}$, normalised to one with respect to the usual Euclidean norm.

The computation of the singular system of the matrix $A_{nm}^{(N,M)}$ is a standard numerical problem and one can use standard routines. The convergence of the approximation can be checked by increasing N and M.

We have first verified the convergence with respect to M for various fixed values of N. The numerical results obtained for values of N_0 between 5 and 25 (N between 2 and 12) indicate that as M_0 is increased from 49 to 97 the first five digits of the first 20 singular values do not change. We give an example in table 1.

This result implies that for an accurate computation of the largest singular values it is sufficient to take $M_0=49$, i.e. to restrict the integral in (1.5) to the interval $[-8, 8]$. This is reasonable because, as we will see, the singular functions associated with the largest singular values are concentrated inside this interval. On the other hand, the singular functions associated with small singular values tend to spread out of this interval and therefore a larger number of sampling points in the object space is required for a correct computation.

The next point is to verify the convergence of the largest singular values (for instance, the first eleven singular values), for $M_0=49$ fixed, when N_0 increases. This is

Table 1. Singular values of $A_{nm}^{(N,M)}$ for $N_0 = 11$ and for various values of M_0, corresponding to the intervals $|y| \leq 2$, 4, 8 and 16.

k	$M_0 = 13$	$M_0 = 25$	$M_0 = 49$	$M_0 = 97$
0	0.603 3185	0.603 3185	0.603 3185	0.603 3185
1	0.256 7505	0.256 7506	0.256 7507	0.256 7506
2	0.107 5034	0.107 5038	0.107 5038	0.107 5038
3	0.040 2823	0.040 2860	0.040 2860	0.040 2860
4	0.023 7160	0.023 7641	0.023 7641	0.023 7641
5	0.019 8000	0.019 8619	0.019 8619	0.019 8619
6	0.009 7259	0.009 9324	0.009 9324	0.009 9324
7	0.004 3345	0.007 6321	0.007 6322	0.007 6322
8	0.002 1716	0.007 3423	0.007 3423	0.007 3423
9	0.000 7147	0.004 0795	0.004 0795	0.004 0795
10	0.000 2587	0.001 8277	0.001 8280	0.001 8280

an important problem from the practical point of view because its solution indicates the minimum number of sampling points in the image space which is required for the computation, within a given accuracy, of a given number of singular values. The results are given in table 2. In the last column we give the values obtained with $N_0 = 97$, $M_0 = 97$. In this case all the digits are correct, as we have verified by increasing the number of sampling points.

Table 2. Singular values of $A_{nm}^{(N,M)}$ for $M_0 = 49$ and for various values of N_0. In the last column the singular values are for $N_0 = M_0 = 97$.

k	$N_0 = 5$, $M_0 = 49$	$N_0 = 7$, $M_0 = 49$	$N_0 = 9$, $M_0 = 49$	$N_0 = 11$, $M_0 = 49$
0	0.602 6863	0.603 2066	0.603 2544	0.603 3185
1	0.256 6841	0.256 7172	0.256 7494	0.256 7507
2	0.106 8757	0.107 0939	0.107 4633	0.107 5038
3	0.039 9315	0.040 1201	0.040 2858	0.040 2860
4	0.013 6988	0.023 1449	0.023 7211	0.023 7641
5	—	0.018 8646	0.019 8424	0.019 8619
6	—	0.007 4985	0.009 9261	0.009 9324
7	—	—	0.005 4959	0.007 6322
8	—	—	0.003 3284	0.007 3423
9	—	—	—	0.004 0795
10	—	—	—	0.001 8280
k	$N_0 = 13$, $M_0 = 49$	$N_0 = 17$, $M_0 = 49$	$N_0 = 21$, $M_0 = 49$	$N_0 = 97$, $M_0 = 97$
0	0.603 3270	0.603 3462	0.603 3530	0.603 3609
1	0.256 7530	0.256 7537	0.256 7539	0.256 7540
2	0.107 5614	0.107 5893	0.107 6001	0.107 6124
3	0.040 2925	0.040 2935	0.040 2937	0.040 2938
4	0.023 7666	0.023 7718	0.023 7735	0.023 7752
5	0.019 8708	0.019 8718	0.019 8720	0.019 8721
6	0.010 0815	0.010 1126	0.010 1251	0.010 1390
7	0.008 0475	0.008 0665	0.008 0674	0.008 0676
8	0.007 6615	0.007 6939	0.007 6968	0.007 6991
9	0.004 2106	0.004 3175	0.004 3228	0.004 3232
10	0.002 7954	0.004 0275	0.004 0466	0.004 0481

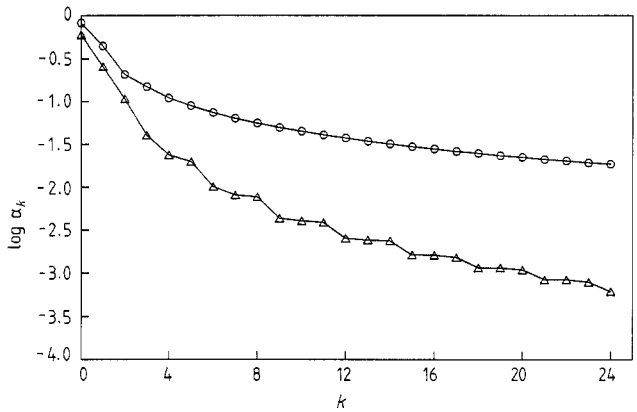

Figure 1. Singular value spectrum of the one-dimensional coherent problem (○) and singular value spectrum of the incoherent problem (△). In both cases $\log \alpha_k$ is plotted as a function of the index k.

As follows from table 2, a satisfactory approximation of the first five singular values is already obtained using nine sampling points in the image space. Analogously the first nine singular values are well approximated using thirteen sampling points.

In figure 1 we compare the singular value spectrum of the incoherent problem with that of the coherent one. We plot the first 25 singular values, obtained with $N_0 = M_0 = 49$. We notice that the singular values of the incoherent problem tend to zero more rapidly than the singular values of the coherent one, i.e. the incoherent problem is more ill posed. This implies, as will be discussed in the next section, that it can be rather difficult to obtain a transfer function which completely fills the available band $[-4\pi, 4\pi]$.

Finally in figure 2 we plot the first eight singular functions $u_k(y)$ obtained with $N_0 = M_0 = 49$. We notice the saturation of the number of zeros inside the central region, a property of the singular functions already remarked in the coherent problem. Starting from the fifth singular function ($k = 4$), all the even singular functions have four zeros inside $(-1, 1)$ while all the odd singular functions have five zeros inside the same interval. We recall that the Rayleigh resolution distance is 1. The points ± 1 are double zeros of the singular functions, as was already remarked in §2. We also observe that for increasing k (and therefore decreasing α_k) the singular functions spread out of the central region, which corresponds to the central lobe of the illuminating beam.

6. The impulse response function

As follows from (2.9), the function $T(y)$, defined in (2.8), is the impulse response function of the super-resolving microscope in the absence of noise. In fact, $T(y)$ is the response to a unit impulse of the system which consists of the confocal microscope, of the detectors for the measurement of the full image, of the computer where the inversion algorithm (2.5) is implemented and of the scanning table. This interpretation is correct only when the full image is detected in the absence of noise and the reconstruction formula (2.5) is used in the absence of round-off errors. In practice,

since the image is noisy, the series (2.5) does not converge and it must be truncated (see I). Moreover we have only a finite set of values of the image $g(x)$. Under these conditions, if the image is sampled at the Nyquist rate and if we use N_0 sampling points for the image, M_0 sampling points for the object and K singular functions for the inversion, then the impulse response function (2.8) is replaced by

$$T_K^{(N,M)}(y) = \sum_{k=0}^{K-1} u_k^{(N,M)}(0) u_k^{(N,M)}(y). \tag{6.1}$$

We notice that, since the singular functions are alternatively even and odd, only the even singular functions contribute to (2.8) or to (6.1).

6.1. *Noise-free data*

We use the results of §3 for determining the impulse response function (2.8), which corresponds to the case of noise-free data.

We first remark that the function

$$P(x, y) = \sum_{k=0}^{+\infty} u_k(x) u_k(y) \tag{6.2}$$

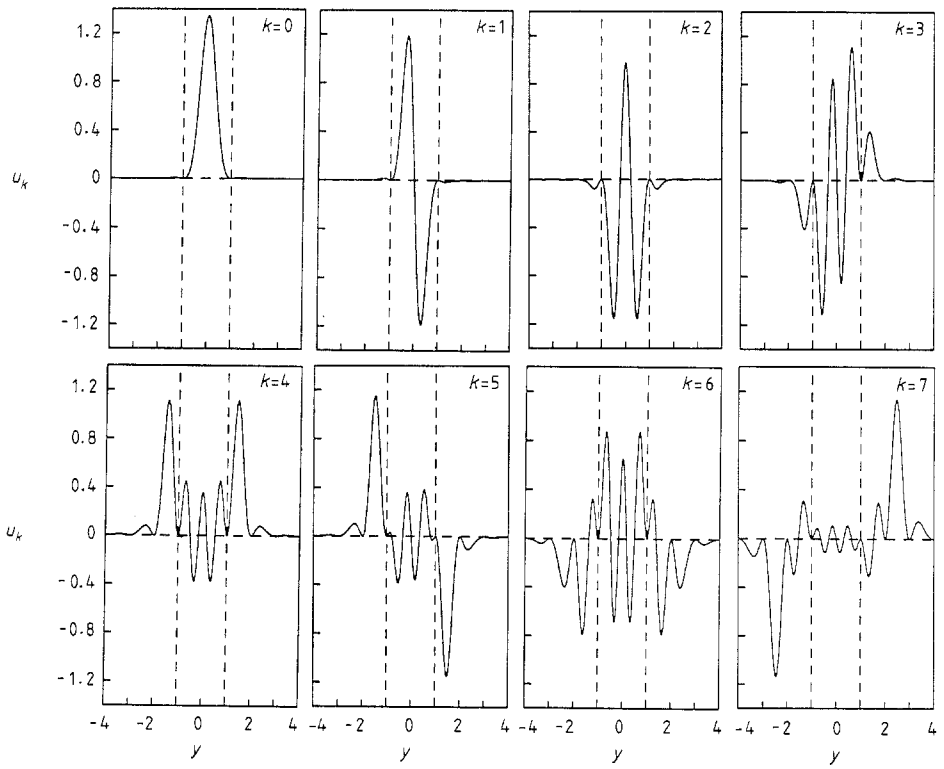

Figure 2. Plot of the first eight singular functions u_k of the one-dimensional incoherent problem.

is the kernel of the projection operator onto the orthogonal complement of the null space of the operator (1.5). Since the functions $u_k(x)$ have bandwidth 4π, from the projection property of the sinc function we have

$$T(y) = 4 \int_{-\infty}^{+\infty} P(x, y) \operatorname{sinc}(4x)\, dx \tag{6.3}$$

and therefore $T(y)$ is the projection onto $N(A)^{\perp}$ of the function

$$f(y) = 4 \operatorname{sinc}(4y). \tag{6.4}$$

If $\phi(y)$ is the projection of $f(y)$ onto $N(A)$ then, from the well known decomposition theorem, we have

$$T(y) = f(y) - \phi(y). \tag{6.5}$$

The Fourier transform of $\phi(y)$, $\hat{\phi}(\omega)$, can be computed by means of (3.13) and (3.16)–(3.21). If we notice that $\hat{f}(\omega) = 1$ when $|\omega| < 4\pi$ (and 0 elsewhere), from (3.16) and (3.17) we have

$$\hat{\alpha}(\omega) = \begin{cases} 1 + \frac{1}{10}\{\lambda - \mu[3 + (1/2\pi)\omega]\} & \omega < 0 \\ 1 - \frac{1}{10}\{\lambda + \mu[3 - (1/2\pi)\omega]\} & \omega > 0. \end{cases} \tag{6.6}$$

Moreover, from (3.20) and (3.21), always in the case $\hat{f}(\omega) = 1$, we obtain

$$I_j = 2\pi \qquad j = 1, 2, 3, 4 \tag{6.7}$$

$$J_j = -5\pi + 2\pi j \qquad j = 1, 2, 3, 4. \tag{6.8}$$

Then, from (3.18) and (3.19) it follows that

$$\lambda = 0 \qquad \mu = \tfrac{15}{4}. \tag{6.9}$$

By substituting in (6.6) we get

$$\hat{\alpha}(\omega) = 1 - \tfrac{3}{8}[3 - (1/2\pi)|\omega|]. \tag{6.10}$$

Since $\hat{\alpha}(\omega)$ is even, $\hat{\phi}(\omega)$ given by (3.13) is also even. Therefore it is sufficient to compute $\hat{\phi}(\omega)$ for $\omega \in (2\pi, 4\pi)$. In such a case $\omega - 2\pi$ belongs to $(0, 2\pi)$ and $\omega - 4\pi$ belongs to $(-2\pi, 0)$. It follows that

$$\hat{\phi}(\omega) = 2\hat{\alpha}(\omega - 2\pi) - \hat{\alpha}(\omega - 4\pi) = 1 - \tfrac{3}{8}[7 - (3/2\pi)\omega] \qquad 2\pi < \omega < 4\pi. \tag{6.11}$$

If we now denote by $\hat{T}(\omega)$ the Fourier transform of $T(y)$, using (6.5), (6.10) and (6.11), we have

$$\hat{T}(\omega) = \begin{cases} \frac{3}{8}[3 - (1/2\pi)|\omega|] & |\omega| < 2\pi \\ \frac{3}{8}[7 - (3/2\pi)|\omega|] & 2\pi < |\omega| < 4\pi. \end{cases} \tag{6.12}$$

In figure 3 we plot the function $\hat{T}(\omega)$ and also the function $\hat{T}_0(\omega)$ which is the Fourier transform of the impulse response function of conventional CSLM, i.e.

$$T_0(y) = \operatorname{sinc}^4(y) \tag{6.13}$$

as follows from (2.10). We notice that, while $\hat{T}_0(\omega) \to 0$ when $|\omega| \to 4\pi$, $\hat{T}(\omega)$ is never zero over the interval $[-4\pi, 4\pi]$ and therefore all the Fourier components of the object in this band are transmitted by super-resolving CSLM, at least in the absence of noise.

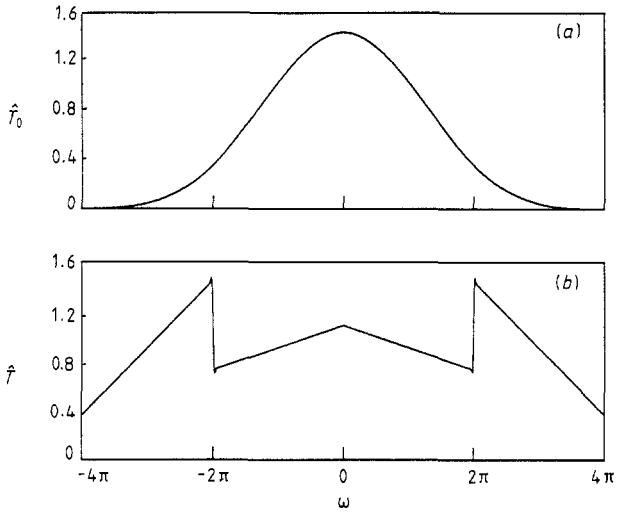

Figure 3. Plots of (*a*) the transfer function $\hat{T}_0(\omega)$ for the conventional confocal scanning microscope and (*b*) the transfer function $\hat{T}(\omega)$ for the noise-free super-resolving microscope.

In figure 4 we plot the impulse response functions $T(y)$ and $T_0(y)$. As one can easily derive from (6.12), $T(y)$ is given by

$$T(y) = \tfrac{9}{2}\,\mathrm{sinc}^2(2y) - \tfrac{3}{4}\,\mathrm{sinc}^2(y) - 3\,\mathrm{sinc}(2y)\,\sin^2(\pi y). \tag{6.14}$$

The super-resolving effect corresponds to the fact that the central peak of $T(y)$ is much narrower than the central peak of $T_0(y)$. This improvement in central resolution is accompanied by decaying side lobes similar to those of the coherent case.

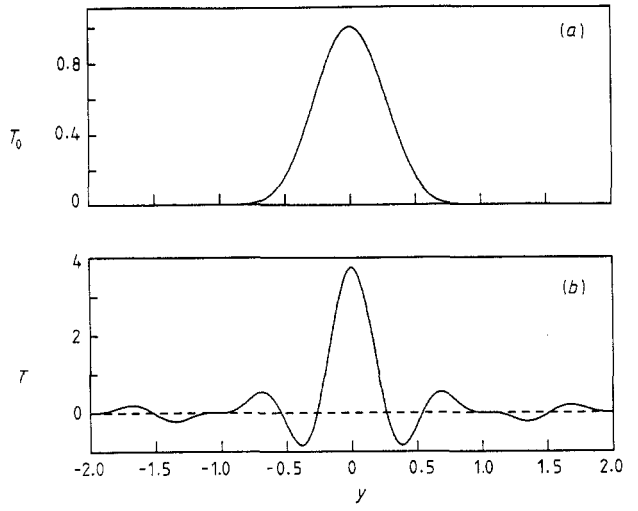

Figure 4. Plots of (*a*) the impulse response function $T_0(y)$ of the conventional confocal microscope and (*b*) the impulse response function $T(y)$ of the noise-free super-resolving microscope. The unit of length is the Rayleigh resolution distance.

6.2. Noisy and discrete data

In the case of noisy data the expansion (2.5) does not in general converge. Then one must consider a truncated singular function expansion. As discussed in I, this approximation is especially good in the case of the recovery of $f^{\dagger}(0)$, since one can use only the singular functions which are large in the central region. Moreover, when we have a finite set of sampled data, we must use the approximate singular functions discussed in §5. Under these conditions the approximate value of the restored object is given by

$$\tilde{f}_K^{(N,M)}(0) = \sum_{k=0}^{K-1} \frac{1}{\alpha_k^{(N,M)}} (\boldsymbol{g}, \boldsymbol{v}_k^{(N,M)}) u_k^{(N,M)}(0) \tag{6.15}$$

and the corresponding impulse response function is given by (6.1).

The stability of the inversion procedure (6.15) is controlled by the *condition number*

$$\mathrm{cond}(K; N, M) = \frac{\alpha_0^{(N,M)}}{\alpha_{K-1}^{(N,M)}}. \tag{6.16}$$

As follows from table 2, for $K = 3$, 5, 7, 9 and 11, the values of the condition number in the case $N_0 = M_0 = 97$ are respectively 5.61, 25.4, 59.6, 78.4 and 149. For smaller values of N_0, M_0 the values of the condition number do not change significantly. This result indicates that if the data are affected by a few per cent noise then eight terms in (6.15) can be taken into account. In this case we have a non-zero contribution only for $k = 0$, 1, 3, 5, 7.

In figure 5 we plot the transfer functions $\hat{T}_K^{(N,M)}(\omega)$, i.e. the Fourier transforms of the functions $T_K^{(N,M)}(y)$, defined in (6.1), for various values of K, in the case $N_0 = M_0 = 97$. We see that for $K \geqslant 49$ the shape of the transfer function is very similar to that of the limit $N = M = \infty$, plotted in figure 3. We also notice that the behaviour of the transfer functions is rather irregular over the band. This means that the image provided by the super-resolving microscope can be strongly distorted. Filtering

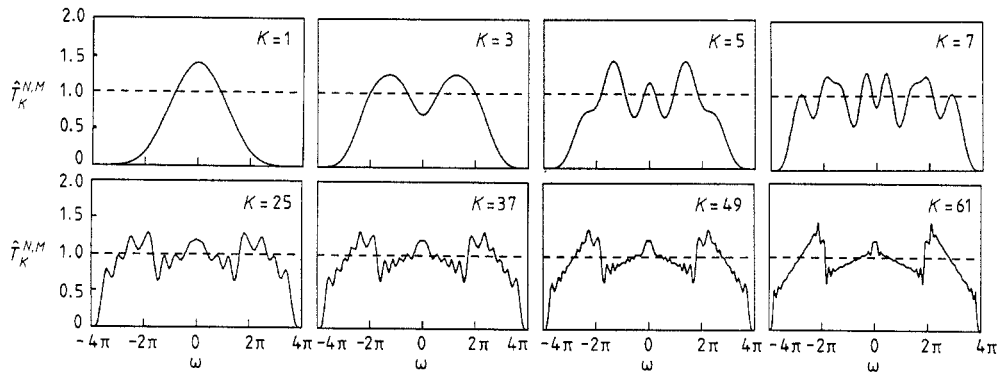

Figure 5. Plot of the transfer functions $\hat{T}_K^{N,M}(\omega)$ for various values of K (number of singular functions used) computed in the case $N_0 = M_0 = 97$.

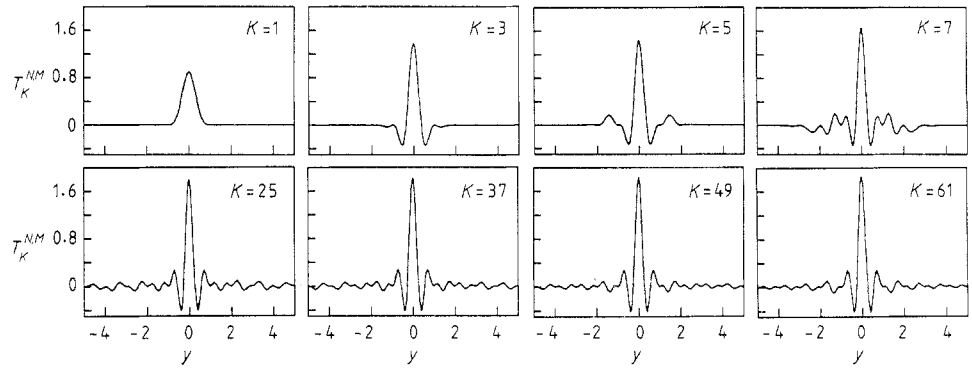

Figure 6. Plot of the impulse response functions $T_K^{N,M}(y)$ for various values of K, computed in the case $N_0 = M_0 = 97$. The unit of length is the Rayleigh resolution distance.

techniques, such as Tikhonov regularisation [6], can be used, however, in order to improve the fidelity of the image in the centre of the band.

In order to estimate the improvement in bandwidth we compare, for example, the transfer function $\hat{T}_K^{(N,M)}(\omega)$, with $K=7$, with the transfer function $\hat{T}_0(\omega)$ of the conventional CSLM (see figure 3). We consider the interval where the transfer function is greater than 0.1. This is a symmetric interval, say $[-\omega_0, \omega_0]$. Then in the case of $\hat{T}_0(\omega)$ we have $\omega_0 = 2.1\pi$ while in the case of $\hat{T}_K^{(N,M)}(\omega)$ we have $\omega_0 = 3.5\pi$. This means that super-resolving CSLM provides a 60% improvement in bandwidth (and therefore a 60% improvement in resolution) with respect to conventional CSLM. The improvement corresponding to $K=9$ and $K=11$ does not differ significantly from the improvement corresponding to $K=7$. These predictions have been verified closely in recent laboratory experiments at King's College, London and this work will be the subject of a separate publication.

In figure 6 we plot the impulse response functions $T_K^{(N,M)}(y)$ for the same values of K as in figure 5.

7. The two-dimensional problem with square pupils

The solution of the one-dimensional problem discussed in the previous sections provides also the solution of the two-dimensional problem in the case of square pupils. In fact, in such a case in (1.1) we have

$$S_1(x) = S_2(x) = S(x) = \operatorname{sinc}(x_1)\operatorname{sinc}(x_2) \tag{7.1}$$

and the singular system of the integral operator

$$(A^{(2)}f)(x) = \int |S(x-y)|^2 |S(y)|^2 f(y)\,dy \tag{7.2}$$

can be obtained from the singular system of the integral operator (1.5) as follows. The singular values of the operator (7.2) are all the possible products of the singular values of the operator (1.5)

$$\alpha_{i,k} = \alpha_i \alpha_k \qquad i, k = 0, 1, 2 \ldots \tag{7.3}$$

and the corresponding singular functions are given by the tensor products of the singular functions of (1.5)

$$u_{i,k}(\mathbf{y}) = u_i(y_1)u_k(y_2) \tag{7.4}$$

$$v_{i,k}(\mathbf{x}) = v_i(x_1)v_k(x_2). \tag{7.5}$$

It is obvious that the singular values with $i \neq k$ have multiplicity 2 while the singular values with $i = k$ have multiplicity 1.

Only the singular functions corresponding to even values of both indices contribute to the reconstruction of the object at the origin. The two-dimensional problem is, however, more ill conditioned than the one-dimensional problem. As we have seen, in the case of $K = 5$ where we use three singular functions with $k = 0, 2, 4$, the condition number is 25.4 in the one-dimensional case. In the two-dimensional case, in order to obtain the same resolution, we must use nine singular functions, corresponding to all the possible pairs of the values 0, 2, 4. But the condition number is now $(25.4)^2 \simeq 645$ and this value could be inconveniently high for the reduction of experimental data, since it would require very large values of the signal-to-noise ratio.

8. Concluding remarks

In §6 we have estimated that super-resolving CSLM can provide an improvement in resolution of about 60% with respect to conventional CSLM. This improvement is much more evident if regularisation techniques [6] are used in order to deconvolve the image provided by super-resolving and/or conventional CSLM. For example, in the case of the Tikhonov regularisation method, the transfer function $\hat{T}_K^{N,M}(\omega)$ is replaced by the following one:

$$\hat{T}_{\alpha,K}^{N,M}(\omega) = \frac{|\hat{T}_K^{N,M}(\omega)|^2}{|\hat{T}_K^{N,M}(\omega)|^2 + \alpha} \tag{8.1}$$

where α is the so-called regularisation parameter whose value is related to the signal-to-noise ratio. Analogously $\hat{T}_0(\omega)$ is replaced by

$$\hat{T}_{\alpha,0}(\omega) = \frac{|\hat{T}_0(\omega)|^2}{|\hat{T}_0(\omega)|^2 + \alpha}. \tag{8.2}$$

In a recent paper Sheppard [14] has proposed an alternative version of super-resolving CSLM. Also in this case one must use many detectors and the signals from the detectors must be appropriately delayed and integrated. One can easily prove that for the one-dimensional problem discussed in this paper the transfer function corresponding to the Sheppard method is given by

$$\hat{T}_1(\omega) = \left(1 - \frac{|\omega|}{4\pi}\right)^2 \qquad |\omega| < 4\pi \tag{8.3}$$

and $\hat{T}_1(\omega) = 0$ elsewhere. Also in this case one can deconvolve the image and this procedure provides a transfer function given by

$$\hat{T}_{\alpha,1}(\omega) = \frac{|\hat{T}_1(\omega)|^2}{|\hat{T}_1(\omega)|^2 + \alpha}. \tag{8.4}$$

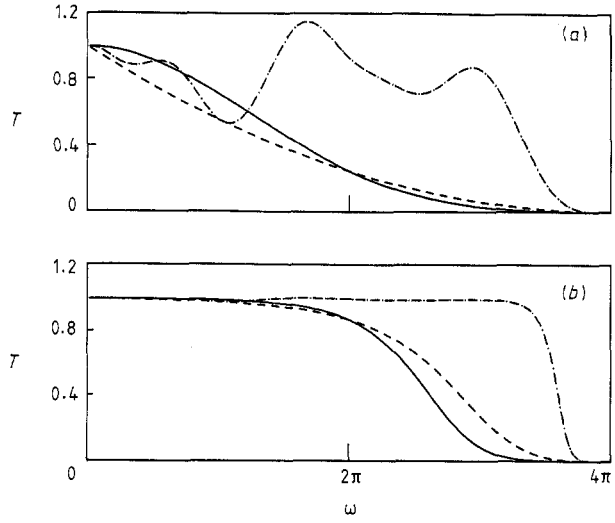

Figure 7. (*a*) Comparison of the transfer functions of the conventional confocal microscope (full curve), of the multidetector microscope proposed by Sheppard (broken curve) and of the super-resolving microscope discussed in this paper (chain curve). (*b*) Regularised versions of the transfer functions plotted in (*a*).

In figure 7 we compare the transfer functions of the various methods. In figure 7(*a*) we plot the unregularised transfer functions and in figure 7(*b*) the regularised ones, assuming a value of the regularisation parameter of the order of 10^{-2}. It is seen that Sheppard's method provides an improvement in resolution with respect to conventional CSLM which is smaller than the improvement provided by the method discussed in this paper.

Acknowledgments

This work has been partly supported by NATO Grant No 463/84, by EEC contract No STE J-0089-3 and by Ministero Pubblica Istruzione, Italy.

References

[1] Bertero M, Brianzi P and Pike E R 1987 Super-resolution in confocal scanning microscopy *Inverse Problems* **3** 195–212

[2] Cox I J, Sheppard C J R and Wilson T 1982 Super-resolution by confocal fluorescent microscopy *Optik* **60** 391–6

[3] Bertero M, De Mol C, Pike E R and Walker J G 1984 Resolution in diffraction limited imaging: IV—The case of uncertain localization or non-uniform illumination of the object *Opt. Acta* **31** 923–46

[4] Brakenhoff G J, van der Voort H T M, van Sprosen E A and Nanninga N 1986 Three-dimensional imaging by confocal scanning fluorescence microscopy *Ann. N.Y. Acad. Sci.* **483** 405–15

[5] Wijnaends van Resandt R W, Marsman H J B, Kaplan R, Davoust J, Stelzer E H K and Stricker R 1985 Optical fluorescence microscopy in three dimensions: microtomoscopy *J. Microsc.* **138** 29–34

[6] Tikhonov A N and Arsenine V Y 1977 *Solutions of Ill-Posed Problems* (Washington, DC: Winston/Wiley)

[7] Reed M and Simon B 1970 *Functional Analysis, Methods of Modern Mathematical Physics* vol. 1 (New York: Academic)
[8] Groetsch C W 1977 *Generalized Inverses of Linear Operators* (New York: Dekker)
[9] Groetsch C W 1984 *The Theory of Tikhonov Regularization for Fredholm Equations of the First Kind* (Boston: Pitman)
[10] Gori F and Guattari G 1985 Signal restoration for linear systems with weighted impulse. Singular value analysis for two cases of low-pass filtering *Inverse Problems* **1** 67–85
[11] Bertero M, De Mol C and Pike E R 1987 Analytic inversion formula for confocal scanning microscopy *J. Opt. Soc. Am.* A **4** 1748–50
[12] Bertero M, Boccacci P, Brianzi P and Pike E R 1987 Inverse Problems in confocal scanning microscopy *Inverse Problems: an Interdisciplinary Study* ed P C Sabatier (New York: Academic) (also *Adv. Electr. Electron Phys.* suppl **19**)
[13] Kato T 1966 *Perturbation Theory for Linear Operators* (Berlin: Springer)
[14] Sheppard C J R 1988 Super-resolution in confocal imaging *Optik* **80** 53–4